

# Zinc Oxide Integrated Wavy Channel Thin Film Transistor Based High Performance Digital Circuits

Amir N. Hanna<sup>1</sup>, *Member, IEEE*, Aftab M. Hussain<sup>1</sup>, *Member, IEEE*, Hesham Omran<sup>2</sup>, Sarah Alsharif<sup>1</sup>, Khaled N. Salama<sup>2</sup>, *Senior Member, IEEE* and Muhammad M. Hussain<sup>1</sup>, *Senior Member, IEEE*

**Abstract**— High performance thin film transistor (TFT) can be a great driving force for display, sensor/actuator, integrated electronics, and distributed computation for Internet of Everything applications. While semiconducting oxides like zinc oxide (ZnO) present promising opportunity in that regard, still wide area of improvement exists to increase the performance further. Here, we show a wavy channel (WC) architecture for ZnO integrated TFT which increases transistor width without chip area penalty, enabling high performance in material agnostic way. We further demonstrate digital logic NAND circuit using the WC architecture and compare it to the conventional planar architecture. The WC architecture circuits have shown 2× higher peak-to-peak output voltage for the same input voltage. They also have 3× lower high-to-low propagation delay times, respectively, when compared to the planar architecture. The performance enhancement is attributed to both extra device width and enhanced field effect mobility due to higher gate field electrostatics control.

**Index Terms**— Wavy channel, Zinc Oxide, Thin Film Transistor, Digital Circuits, NAND.

## I. INTRODUCTION

For more than a decade, amorphous metal oxide semiconductors (AOS) have been explored as promising candidates for flexible, transparent, and large-area displays and electronics [1, 2]. N-type oxides are particularly of interest due to their higher field-effect mobility (10 cm<sup>2</sup>/V.s) compared to p-type oxides [2, 3]. Amorphous Indium Gallium Zinc Oxide (In-Ga-Zn-O) mobility was optimized to ~20 cm<sup>2</sup>/V.s for Indium (In) rich films [4]. For display applications, field effect mobility in excess of 20 cm<sup>2</sup>/V.s had been previously set as a benchmark for future Active Matrix Oxide Light Emitting Diode (AMOLED) displays [5]. An even higher mobility benchmark of 80 cm<sup>2</sup>/V.s mobility is set to be on par with low temperature poly silicon (LTPS) technology [6]. Recent material development for n-type oxides has led to field effect mobility in excess of 100 cm<sup>2</sup>/V.s for Zinc Oxynitride (ZnON) films [7], which was even higher than InGaO<sub>3</sub>(ZnO)<sub>5</sub> single crystalline films [8]. However, for beyond display large-area macro-electronics applications such as: digital logic

applications for distributed computing and sensors/actuators integrated electronics for Internet of Everything applications, optimization of TFT switching speed becomes an important benchmark. Field effect transistor transit frequency,  $f_T$ , is typically used to quantify the speed of the devices. Expression for transit frequency is given by [9]:

$$f_T = \frac{g_m}{2 \times \pi \times C_{ox}} \sim \frac{\mu \times (V_{GS} - V_T)}{2 \times \pi \times L_{ch}^2} \quad (1)$$

Where,  $g_m$  is the transconductance,  $C_{ox}$  is the oxide gate capacitance,  $\mu$  is the carrier mobility,  $L_{ch}$  is the channel length, and  $(V_{GS} - V_T)$  is the gate overdrive voltage of the TFT, where  $V_T$  is the threshold voltage. Although material related properties such as channel mobility,  $\mu$ , and oxide dielectric capacitance,  $C_{ox}$ , are still relevant for optimization of  $f_T$ , other parameters in equation (1) are still critical. For a given semiconductor/dielectric gate stack, besides  $V_T$  engineering, gate length ( $L_g$ ) scaling has traditionally been the major approach for improving  $f_T$ . There are two main approaches for  $L_g$  scaling: (i) top down lithographic scaling shown for amorphous In-Ga-Zn-O (IGZO) TFT down to  $L_g$  of 0.18  $\mu\text{m}$ . This approach; however, is both expensive and suffers from sensitivity of TFT properties such as saturation mobility to processing variations in the gate-to-contact spacing, and the shape of the active area [10]; and (ii) non-lithographically defined gate length using vertical channel TFT architecture [11]. Although, it is less expensive compared to the first approach, the TFT properties suffer immensely from both gate leakage and gate-to-source/drain overlap capacitance. Finally,  $L_g$  scaling is known to induce negative  $V_T$  shift which in return increases the OFF current,  $I_{OFF}$ , value and degrades the device static power consumption [12]. Therefore, we showed a novel approach, which improves  $I_{ON}$  per unit chip area by increasing the device width vertically without extra chip area penalty, as well as, enhances the field effect mobility,  $\mu_{FE}$ , and thus  $g_m$  per unit device width due to better electrostatics, as reported in our previous works [13-17]. This allows boosting performance of the smallest reliable  $L_g$  without changing  $V_T$  or  $I_{OFF}$ .

## II. TFT AND CIRCUIT CHARACTERIZATION

The idea behind the device is to introduce corrugations to the substrate using anisotropic etching to increase the device width without extra chip area penalty. Details of device fabrication can be found in our previous work [17]. Fig. 1(a) shows an optical image of  $L_g = 10 \mu\text{m}$  device. Fig. 1(b) shows a side view

This publication is based upon work supported by the King Abdullah University of Science and Technology (KAUST) Office of Sponsored Research (OSR) under Award No CRG-1-2012-HUS-008.

<sup>1</sup>Authors are with the Integrated Nanotechnology Lab and Integrated Disruptive Electronic Applications (IDEA) Lab, <sup>2</sup>Sensors Lab, Electrical Engineering, Computer Electrical Mathematical Science and Engineering Division of King Abdullah University of Science and Technology (KAUST), Thuwal 23955-6900, Saudi Arabia (e-mail: muhammadmustafa.hussain@kaust.edu.sa).

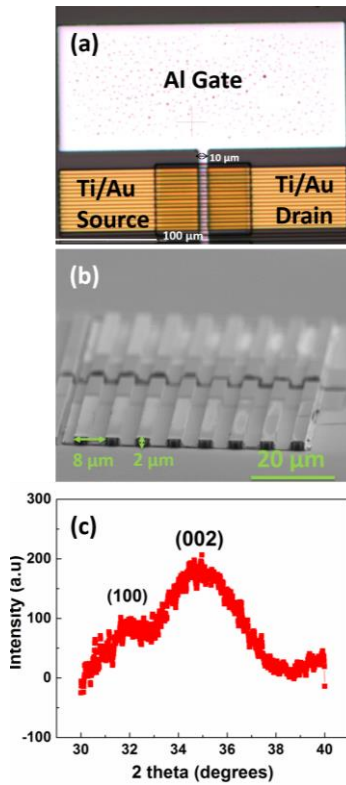


Fig. 1 (a) Digital image showing  $L_g=10\ \mu\text{m}$  device, and (b) Titled view SEM image of the device in (a) showing  $4\ \mu\text{m}$  wide fin, where the fin height is  $2\ \mu\text{m}$ , and the fin pitch is  $8\ \mu\text{m}$  pitch ( $4\ \mu\text{m}$  1-1 device). (c) Grazing incidence XRD of the ZnO film showing weak Wurtzite peaks.

SEM image of WC TFT which we refer to as  $4\ \mu\text{m}$  1-1 device, showing  $4\ \mu\text{m}$  wide fin-like feature, with  $2\ \mu\text{m}$  fin height and  $8\ \mu\text{m}$  fin pitch. The device has 50% larger width when compared to a planar device consuming the same chip area. Fig. 1(c) shows Grazing Incidence X-ray Diffraction (GIXRD) pattern of the ZnO film, showing a weak (100) and a dominant (002) Wurtzite peaks, which have been reported in the literature for ALD films deposited at similar conditions [18, 19]. The film crystallinity was further checked with SEM images, which showed rice-like grains with sizes  $< 20\ \text{nm}$ , confirming the film is polycrystalline.

Figs. 2(a, b) show the transfer and output characteristics of  $L_g = 10\ \mu\text{m}$  device, the WC and planar devices have  $V_T$  values of 2.7 and 2V, respectively. Output characteristics show that the WC TFT has  $2\times$  the output current of the planar TFT consuming the same chip area, where the WC and planar TFTs have  $I_{DS}$  of 1.8 mA and 0.9 mA, respectively, at  $V_{GS} = 10\text{V}$ . No increase in the  $I_{OFF}$  value can be seen in Fig. 2(a), which is desirable for reducing the static power consumption. The increase in the drive current is not only proportional to the 50% extra device width, rather it had boost up from other sources due to the device architecture. Hence, analyzing the saturation mobility of both devices,  $\mu_{sat}$ , it was found that WC devices had a peak value of  $7.1\ \text{cm}^2/\text{V}\cdot\text{s}$  while planar devices had a peak value of  $4.8\ \text{cm}^2/\text{V}\cdot\text{s}$ , as shown in Fig. 2(c). This amounts to  $\sim 50\%$  higher mobility for WC TFTs, when compared to the planar counterparts. The calculation was done taken into account the 50% extra device width,  $W_{extra}$ , of the WC TFT according to the saturation mobility expression [20]:

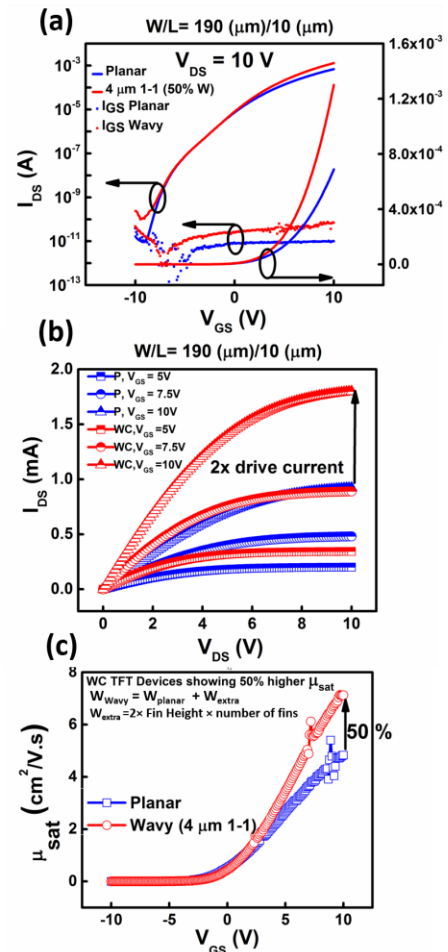


Fig. 2 (a) Transfer, and (b) output characteristics of  $L_g=10\ \mu\text{m}$  devices. (c) WC devices showing 50% higher saturation mobility,  $\mu_{sat}$ .

$$\mu_{sat} = \left(\frac{2L_g}{W}\right) \left(\frac{1}{C_{ox}}\right) \left(\frac{d\sqrt{I_{DS}}}{dV_{GS}}\right) \quad (2)$$

Where  $W$  is the device width. This means that WC device has 50% higher transconductance per unit device width, which cannot be accounted for by  $W_{extra}$ . Therefore, in order to explain the enhancement in field effect mobility, the device geometry and electrostatics need to be analyzed. When analyzing the fin cross-section, we found that the device has a zigzag like sidewall gate stack, as shown in Figs. 3(a, b). This is due to the etch profile of the anisotropic reactive ion etching that depends on two steps of: i) side wall passivation and ii) subsequent etching, which gives rise to the sidewall scallops. Hence, to evaluate the effect on charge accumulation in the channel due to the gate metal zigzag profile, a COMSOL<sup>TM</sup> simulation of the device electrostatics was performed to scale of the SEM image in Figs. 3(b). The ZnO material parameters were taken from the literature for polycrystalline ZnO films [21]. Simulation has shown a  $2.3\times$  higher electric field in the around the sharp corner of the zigzag gate as shown in Fig. 3(c), which, as a result, led to 15% higher carrier concentration as shown in Fig. 3(d) compared to a planar gate, when biased at  $V_{GS} = 10\text{V}$ . Fig. 2(c) shows that  $\mu_{sat}$  is higher for WC TFT when  $V_{GS} > 5\text{V}$ , which shows gate-field dependent mobility enhancement.

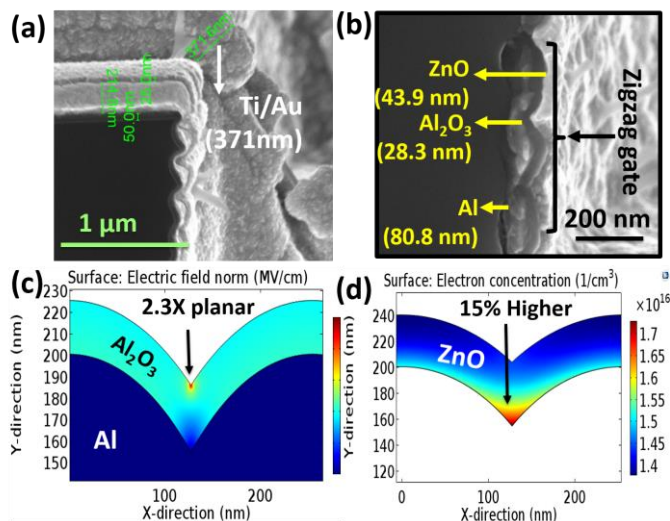


Fig. 3 (a) Sidewall cross-section showing thickness of various device parameters, and (b) Zoomed in image of the gate stack. COMSOL simulation of (c) Surface Electric Field norm in  $\text{Al}_2\text{O}_3$  gate dielectric and (d) electron concentration in the ZnO channel, both to scale with (b) biased at  $V_{GS} = 10\text{V}$ .

Modelling study has shown that in a polycrystalline ZnO TFT, nanoscale grains induce a strong overlap of the double Schottky barriers with a higher activation energy in the crystallite and a lower barrier potential in the grain boundary [21]. Here the grain boundary Schottky Barrier Height (SBH) is modulated by the gate field [21], which was confirmed experimentally as well [22]. Hence the  $2.3\times$  higher field in the channel could qualitatively explain why WC devices have a higher field effect mobility, compared to planar devices. The simulation results also have relevance for AOS based TFTs because of gate field dependent effective mobility. Here percolation transport mechanism dominates transport at high gate fields, in which the field effect mobility,  $\mu_{FE}$ , is controlled by percolation through non-localized states through the path of least resistance among the potential barriers whose height is controlled by the gate field [23]. Thus, we believe the WC architecture could enhance  $\mu_{FE}$  for AOS based TFTs.

We wanted to measure the effect of the new architecture on leveraging higher performance for the same channel material, when compared to the conventional planar architecture. This is the case since the increase in the current is not just proportional to the increase in device width. Hence, the WC devices should manifest faster switching since they have larger transconductance,  $g_m$ , per device width. Thus, to compare the circuit performance of the new architecture, we have chosen NAND circuit for the comparison between the two architectures using NMOS logic design.

Fig. 4(a) shows NAND circuit design using transistor with  $L_g = 10\ \mu\text{m}$ , drive transistor widths of  $600\ \mu\text{m}$  and pull-up transistor width of  $30\ \mu\text{m}$ . The two devices in comparison occupy the same chip area. The two gates are driven by the same input square wave of  $10\ \text{V}$  peak-to-peak voltage, i.e.  $V_{input\ Low} = 0\text{V}$  and  $V_{input\ High} = 10\text{V}$ , one NAND input is driven with a frequency  $f = 200\ \text{Hz}$ , and the other with  $100\ \text{Hz}$ . Figs. 4(b,c) show the output of the WC and planar NAND circuit, where WC NAND circuit has shown more than  $2\times$  increase in

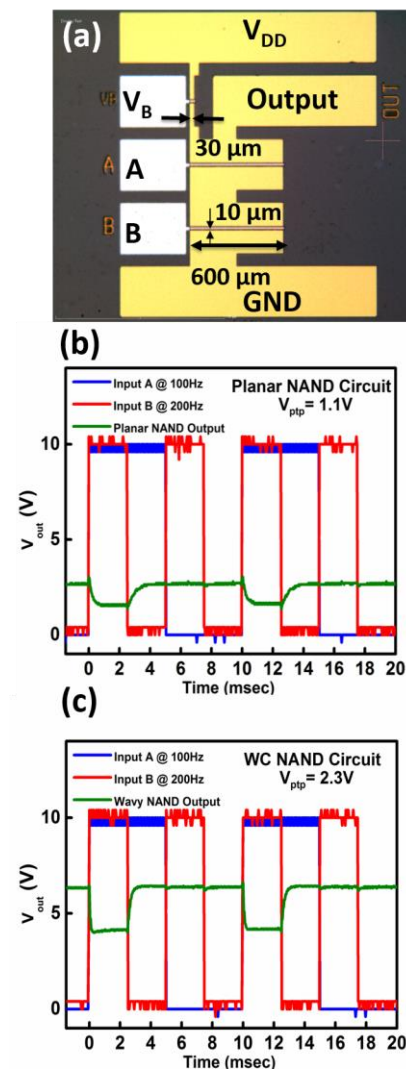


Fig. 4 (a) Digital image of  $L_g = 10\ \mu\text{m}$  NAND circuit, showing device dimensions. (b-c) Comparison showing  $100\%$  higher  $V_{out\ ptp}$  for WC NAND and  $3\times$  lower high-to-low propagation delay  $t_{PHL}$ .

the output peak-to-peak voltage,  $V_{out\ ptp}$ , when compared to the planar circuit. It could also be noticed that the high-to-low propagation delay time,  $t_{PHL}$ , was shorter for WC NAND circuit when compared to the planar counterpart. The propagation delay time is defined as the maximum time from the input crossing  $50\%$  to the output crossing  $50\%$  [24]. The  $t_{PHL}$  of the fabricated circuits were  $120$ , and  $40\ \mu\text{s}$  for planar and WC NAND circuits, respectively, thus showing  $3\times$  lower  $t_{PHL}$  for WC NAND.

### III. CONCLUSION

We have presented wavy architecture based ZnO integrated TFT based digital logic circuit components. NAND WC circuits has shown  $2\times$   $V_{out\ ptp}$  and  $3\times$  faster high-to-low propagation delay when compared to conventional planar circuits, thus enabling high performance digital logic circuits even for low mobility channel materials.

## REFERENCES

- [1] K. Nomura, H. Ohta, A. Takagi, T. Kamiya, M. Hirano, and H. Hosono, "Room-temperature fabrication of transparent flexible thin-film transistors using amorphous oxide semiconductors," *Nature*, vol. 432, pp. 488–492, Nov. 2004. DOI: 10.1038/nature03090.
- [2] E. Fortunato, P. Barquinha, and R. Martins, "Oxide semiconductor thin-film transistors: A review of recent advances," *Adv. Mater.*, vol. 24, no. 22, pp. 2945–2986, May. 2012. DOI: 10.1002/adma.201103228.
- [3] T. Kamiya, K. Nomura, and H. Hosono, "Present status of amorphous In–Ga–Zn–O thin-film transistors," *Sci. Technol. Adv. Mater.*, vol. 11, no. 4, pp. 044305, Sep. 2010. DOI: 10.1088/1468-6996/11/4/044305.
- [4] J. K. Jeong, J. H. Jeong, H. Yang, J. Park, Y. Mo, and H. Kim, "High performance thin film transistors with cosputtered amorphous indium gallium zinc oxide channel," *Appl. Phys. Lett.*, vol. 91, no. 11, pp. 113505, Sep. 2007. DOI: 10.1063/1.2783961.
- [5] T. Arai, and T. Sasaoka, "Emergent Oxide TFT Technologies for Next-Generation AM-OLED Displays," *SID International Symposium Digest of Technical Papers*, vol. 42, no. 1, pp. 710–713, Aug. 2012. DOI: 10.1889/1.3621424.
- [6] J. Kwon, and J. Jeong, "Recent progress in high performance and reliable n-type transition metal oxide-based thin film transistors," *Semicond. Sci. Technol.*, vol. 30, no. 2, pp. 1–16, Jan. 2015. DOI: 10.1088/0268-1242/30/2/024002.
- [7] E. Lee, A. Benayad, T. Shin, H. Lee, D. Ko, T. Kim, K. Son, M. Ryu, S. Jeon, and G. Park, "Nanocrystalline ZnON; High mobility and low band gap semiconductor material for high performance switch transistor and image sensor application," *Sci. Rep.*, vol. 4, no. 4948, pp. 1–7, May. 2014. DOI: 10.1038/srep04948.
- [8] K. Nomura, H. Ohta, K. Ueda, T. Kamiya, M. Hirano, and H. Hosono, "Thin-Film Transistor Fabricated in Single-Crystalline Transparent Oxide Semiconductor," *Science*, vol. 300, no. 5623 pp. 1269–1272, May. 2003. DOI: 10.1126/science.1083212.
- [9] S. Sze, "Ch.6: JFET and MESFET," in *Physics of Semiconductor Devices*, 2<sup>nd</sup> ed., New York: Wiley, 1981, pp. 343. DOI: 10.1002/0470068329.
- [10] S. Jeon, A. Benayad, S. Ahn, S. Park, I. Song, C. Kim, and U. Chung, "Short channel device performance of amorphous InGaZnO thin film transistor," *Appl. Phys. Lett.*, vol. 99, no. 8, pp. 082104, Aug. 2011. DOI: 10.1063/1.3623426.
- [11] L. Petti, P. Aguirre, N. Münzenrieder, G. Salvatore, C. Zysset, A. Frutiger, L. Büthe, C. Vogt, and G. Tröster, "Mechanically flexible vertically integrated a-IGZO thin-film transistors with 500 nm channel length fabricated on free standing plastic foil" Presented at *IEEE Int. Elect. Devices Meet. 2013* [Online], Available: [http://ieeexplore.ieee.org/xpls/abs\\_all.jsp?arnumber=6724609](http://ieeexplore.ieee.org/xpls/abs_all.jsp?arnumber=6724609). DOI: 10.1109/IEDM.2013.6724609.
- [12] H. Hsieh, and C. Wu, "Scaling behavior of ZnO transparent thin-film transistors," *Appl. Phys. Lett.*, vol. 89, no. 4, pp. 041109, Jul. 2006. DOI: 10.1063/1.2235895.
- [13] A. Hanna, M. Ghoneim, R. Bahabry, A. Hussain, and M. Hussain, "Zinc oxide integrated area efficient high output low power wavy channel thin film transistor," *Appl. Phys. Lett.*, vol. 103, no. 22, pp. 224101, Nov. 2013. DOI: 10.1063/1.4836235.
- [14] A. Hanna, G. Sevilla, M. Ghoneim, Af. Hussain, R. Bahabry, A. Syed, and M. Hussain, "Wavy channel thin film transistor architecture for area efficient, high performance and low power displays" *Phys. Status Solidi RRL*, vol. 8, no. 3, pp. 248–251, Dec. 2013. DOI: 10.1002/pssr.201470515.
- [15] A. Hanna, M. Ghoneim, R. Bahabry, A. Hussain, H. Fahad, and M. Hussain, "Area and Energy Efficient High-Performance ZnO Wavy Channel Thin-Film Transistor," *IEEE Trans. Electron Devices*, vol. 61, no. 9, pp. 3223–3228, Sep. 2014. DOI: 10.1109/TED.2014.2336863.
- [16] A. Hanna, A. Hussain, M. Ghoneim, J. Rojas, G. Sevilla, and M. Hussain, "Wavy Channel TFT Architecture for High Performance Oxide Based Displays" *ECS Trans.*, vol. 67, no. 1, pp. 191–198, 2015. DOI: 10.1149/06701.0191ecst.
- [17] A. Hanna, A. Hussain, and M. Hussain, "Wavy Channel architecture thin film transistor (TFT) using amorphous zinc oxide for high-performance and low-power semiconductor circuits" Presented at *IEEE Dev. Res. Conf. 2015* [Online] Available: [http://ieeexplore.ieee.org/xpls/abs\\_all.jsp?arnumber=7175633](http://ieeexplore.ieee.org/xpls/abs_all.jsp?arnumber=7175633). DOI: 10.1109/DRC.2015.7175633
- [18] S. Jeon, S. Bang, S. Lee, S. Kwon, W. Jeong, H. Jeon, H. Chang, and H. Park, "Structural and Electrical Properties of ZnO Thin Films Deposited by Atomic Layer Deposition at Low Temperatures" *J. Electrochem. Soc.*, vol. 155, no. 10, pp. H738–H743, Aug. 2008. DOI: 10.1149/1.2957915
- [19] B. Oh, Y. Kim, H. Lee, B. Kim, H. Park, J. WooHan, G. Heo, T. Kim, K. Kim and D. Seo, "High-performance ZnO thin-film transistor fabricated by atomic layer deposition" *Semicond. Sci. Technol.*, vol. 26, pp. 085007 (1–5), May. 2011.
- [20] D. Schroder, "Ch8: Mobility," in *Semiconductor material and device characterization*, 3rd ed., New Jersey: John Wiley & Sons, 2006, pp. 502. DOI: 10.1002/0471749095. Ch. 8.
- [21] F. Hussain, J. Nishii, S. Takagi, A. Ohtomo, T. Fukumura, H. Fujioka, H. Ohno, H. Koinuma, and M. Kawasaki, "Modeling and simulation of polycrystalline ZnO thin-film transistors," *J. Appl. Phys.*, vol. 94, no. 12, pp. 7768–7777, Oct. 2003. DOI: 10.1063/1.1628834.
- [22] R. Hoffman, "ZnO-channel thin-film transistors: Channel mobility," *J. Appl. Phys.*, vol. 95, no. 10, pp. 5813–5819, May. 2004. DOI: 10.1063/1.1712015. DOI: 10.1088/0268-1242/26/8/085007.
- [23] S. Lee, K. Ghaffarzadeh, A. Nathan, J. Robertson, S. Jeon, C. Kim, I. Song, and U. Chung, "Trap-limited and percolation conduction mechanisms in amorphous oxide semiconductor thin film transistors," *Appl. Phys. Lett.*, vol. 98, no. 20, pp. 203508, May. 2011. DOI: 10.1063/1.3589371.
- [24] N. Weste, and D. Harris, "Ch3: SPEED," in *Integrated Circuit Design*, 4<sup>th</sup> ed., New York: Pearson, 2010, pp. 99.